

# Optimal grid size for precipitators using finite difference method based on full multi-grid method

Mohamed A. Abouelatta\*, A.M. Omar\*, Sayed Ward

Shoubra Faculty of Engineering, Benha University, 108 Shoubra St., Cairo, Egypt

## ARTICLE INFO

### Keywords:

Precipitators  
Finite difference method  
The full multigrid method

## ABSTRACT

The paper presents a novel approach for tracking the optimal grid size of the computational domain for modeling the corona problem within the wire-duct precipitators, which in turn helps in decreasing the experimental efforts. The Finite Difference Method (FDM) is used to model the corona problem using the full multi-grid method (FMG) as a powerful convergent iterative solution for Poisson equation particularly on finer computational domains. The full multi-grid method is examined against successive over relaxation (SOR) strategy and the latter is effectively transcendent in terms of timing performance. Indeed, using finer grids is a double ended weapon; on one hand it reduces the truncation error of the Finite Difference Method which reflects in getting more accurate view for the corona problem in precipitators. While on the other hand, the round off error will be increased which might give un-accurate results. Accordingly, the issue of choosing the optimal grid size arises. The full multi-grid method tracked the optimal grid size that gives the appropriate results for the potential and current density that well matched the previous published experimental measurements.

## 1. Introduction

The advance in technology is met by an increase in the generation of electrical power. The gas streams resulted from some industrial power plants contain particles that would cause air pollution [1–3]. To reduce the harmful effects from air pollution, the need for a device with high collecting efficiency is a must. Among these devices, the electrostatic precipitators have a significant effect in decreasing and controlling the air pollution results from these power plants [4]. The basic idea of precipitators is charging the inlet gas stream with ions and these particles will deposit on the ground plate and then by rapping process, these particles can be removed. Precipitators are widely used in many technologies like gold recovery technology [5,6]. This technology produces sulfuric acid which can be removed by precipitators. In addition, thermal power plants produce fly ashes which can be controlled by precipitators [7]. Generally, precipitators are of great importance to overcome the harmful effects resulting from the increasing technologies.

The operational performance of the electrostatic precipitators is greatly affected by its electrical properties. Accordingly, several numerical methods are implemented to evaluate such performance. This methods includes Finite Difference Method (FDM) [2,8,9], Finite Element Method coupled with Finite Difference Method [10], Boundary

Element Method (BEM) coupled with the method of characteristics [11], Boundary Element Method combined with Finite Difference Method [12], Finite Element Method (FEM) [13], Charge Simulation Method (CSM) [14], Finite Element Method combined with the method of characteristics [15–17], and Finite Volume Method [18,19]. These numerical techniques give a prediction of the performance of precipitators by calculating the voltage–current (V/I) density curves. They deal with different design parameters such as the wire radius, the distance between the two collecting plates, the height of the wire above the grounded plate in addition to the environmental conditions.

The Finite Difference Method solves both Poisson equation and continuity equation by finite difference equations to model the corona problem. These equations are simplified by truncating the higher order terms that might result in high truncation error, which can be minimized by using finer grids. Among the classical iterative methods used to solve the finite difference equations are Jacobi method, Gauss-Seidel method, and successive over-relaxation method (SOR). In order to reach a certain convergence by these methods, they need order of ( $N^2$ ) iterations, where  $N$  is the linear grid size, which is acceptable on dealing with coarse grids, but when the grids become finer, these methods are time consuming [2,20]. Therefore, seeking for an efficient iterative method is of a great interest.

In order to increase the convergence rate of the classical iterative

\* Corresponding author.

E-mail addresses: [moh\\_an1@yahoo.com](mailto:moh_an1@yahoo.com) (M.A. Abouelatta), [ahmad\\_m\\_omar@yahoo.com](mailto:ahmad_m_omar@yahoo.com) (A.M. Omar).

methods, the multi-grid method is introduced [21,22]. The multi-grid method deals with different grids of various sizes. They smooth the high frequency error by using any of the classical iterative techniques, and reducing the low frequency errors by a coarse-grid correction method [20]. The multi-grid method changes the fine grid into coarser grid which can be solved by Gauss-Seidel and then by grid transfer operators, the solution is used as improved initial values for the finer meshes.

The main items of the multi-grid method are smoothers, restriction and prolongation [20]. The multi-grid method can reduce the high frequency error by smoothers. One of the grid transfer operators is restriction in which the defect in the residuals is mapped from the smoothed fine mesh to a coarser mesh. There are different restriction schemes including straight injection, half weighting and full weighting [2,20]. The other mesh transfer operator is interpolation. It can be implemented by bilinear interpolation, in which the value of each new mesh node is computed based on the mean of all existing neighboring nodes. There are various schemes for implementing the multigrid method such as the two-grid method, V-cycle, W-cycle and the full multigrid method [20].

Generally, two basic problems of using finer grids are faced. The first is the excessive computational time if, the finite difference equations is solved by any of the classical iterative techniques. The second is the round off error. The first can be fixed and treated well by using multi-grid methods [2,20]. The second can be fixed by tracking the optimal grid. Optimality here means choose a fine grid that grantee both low truncation error and round off error, which is the main issue of the present paper.

In this paper, the finite difference method is implemented to choose the optimal grid size for the computational domain to solve the corona problem within the wire-duct precipitators in clean air. To follow up the optimal grids, the finite difference method should deal with finer grids. So, the full multi-grid method (FMG) is used as an iterative solution for the finite difference equations. Firstly, the full multi-grid method is examined against successive over relaxation (SOR) method for different relaxation factors with respect to the timing performance, and the full multi-grid method confirms more efficiency. Secondly, the finite difference method with the help of the full multi-grid method is implemented to choose the optimal grid size for different geometries of precipitators. By choosing the optimal grid size for a certain precipitator the researchers can predict the effect of the variation of different design parameters on the performance of the precipitator. Finally, the effect of changing the applied voltage, the spacing between wires and the wire height above the ground is discussed.

## 2. Governing equations and boundary conditions

Two basic equations are used to model the corona problem during the steady-state conditions. They are Poisson and current continuity equations [2,9];

$$\nabla^2 V = -\frac{\rho}{\epsilon_0} \quad (1)$$

Where  $V$  is the applied potential difference,  $\rho$  is the ionic space charge density, and  $\epsilon_0$  is the permittivity of the free space.

Where, the electric field,  $E$ , and the corona current density,  $j$ , are given by:

$$E = -\nabla V \quad (2)$$

$$\nabla \cdot j = 0 \quad (3)$$

$$j = \rho k E \quad (4)$$

Where,  $k$  is the ion mobility in  $m^2/Vs$ .

Eq.(1), and Eq.(2) are Poisson and current continuity equations respectively.

Due to the symmetry of the problem, only one quarter of the computational domain is considered. The area under study in the

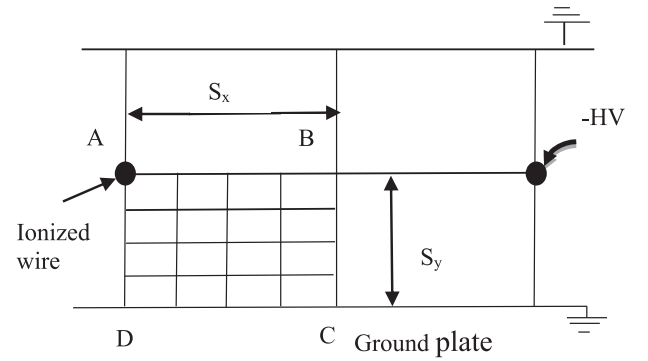


Fig. 1. Wire-duct precipitator.

precipitator is shown in Fig. 1, and the following assumptions are considered [2,9];

- 1 At point A,  $\rho = \rho_0$ , and the voltage equals to the applied voltage.
- 2  $E_x$  at points A, B, and along lines BC, CD, and AD, equals zero.
- 3  $E_y$  equal zero at points A and B, and along line AB
- 4 Along line CD, the potential equals zero.

## 3. Solution of continuity equation

Assuming a single and constant "apparent" mobility representing the motion of all the charge carriers, and substituting in the continuity Eq. (3) by Eq. (4) using backward finite difference:

$$\left(\frac{a_x a_y}{\epsilon_0}\right) \rho_{i,j}^2 + (a_x E_y + a_y E_x) \rho_{i,j} - (a_x E_y \rho_{i-1,j} + a_y E_x \rho_{i,j-1}) = 0 \quad (5)$$

Where  $E_x$ ,  $E_y$  are the electric field intensities along the x and y directions respectively,  $a_x$ ,  $a_y$  are the incremental spacing along x and y directions respectively.

By solving Eq. (5), the charge density at any point,  $\rho$  (i, j) in the grid can be computed.

At point A, the charge density,  $\rho_0$ , can be calculated from [2,9]:

$$\rho_0 = \frac{2S_x j_p}{\pi k r f (30\delta + 9\sqrt{\frac{\delta}{r}})} \times 10^{-3} \quad (6)$$

The air density factor,  $\delta$ , is given by [23]:

$$\delta = \frac{298p}{760(t + 273)} \quad (7)$$

Where  $f$  is the surface roughness factor,  $r$  is the radius of the ionized wire (cm),  $j_p$  is the average current density on the plate, and  $S_x$  is the half spacing between the ionized wires,  $t$  is the temperature in Celsius and  $p$  is the pressure in mmHg.

F. W. Peek's formula [23] has been adopted in Eq. (6), although accurate estimation of the corona inception field still remains an interesting subject for investigation [24–28].

## 4. Solution of Poisson equation

Using the assumptions mentioned before, the finite difference method is used to solve the 2-D corona problem on a rectangular domain, Fig. 2. So, Eq. (1) can be formulated using finite difference method using successive over relaxation method as iterative solver from:

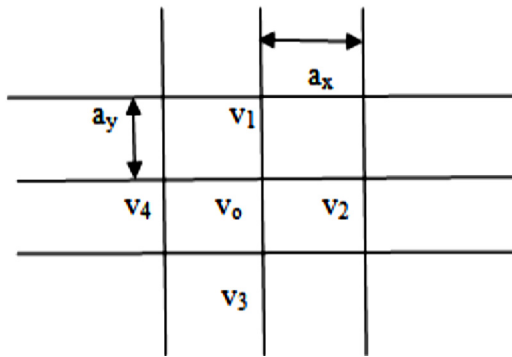
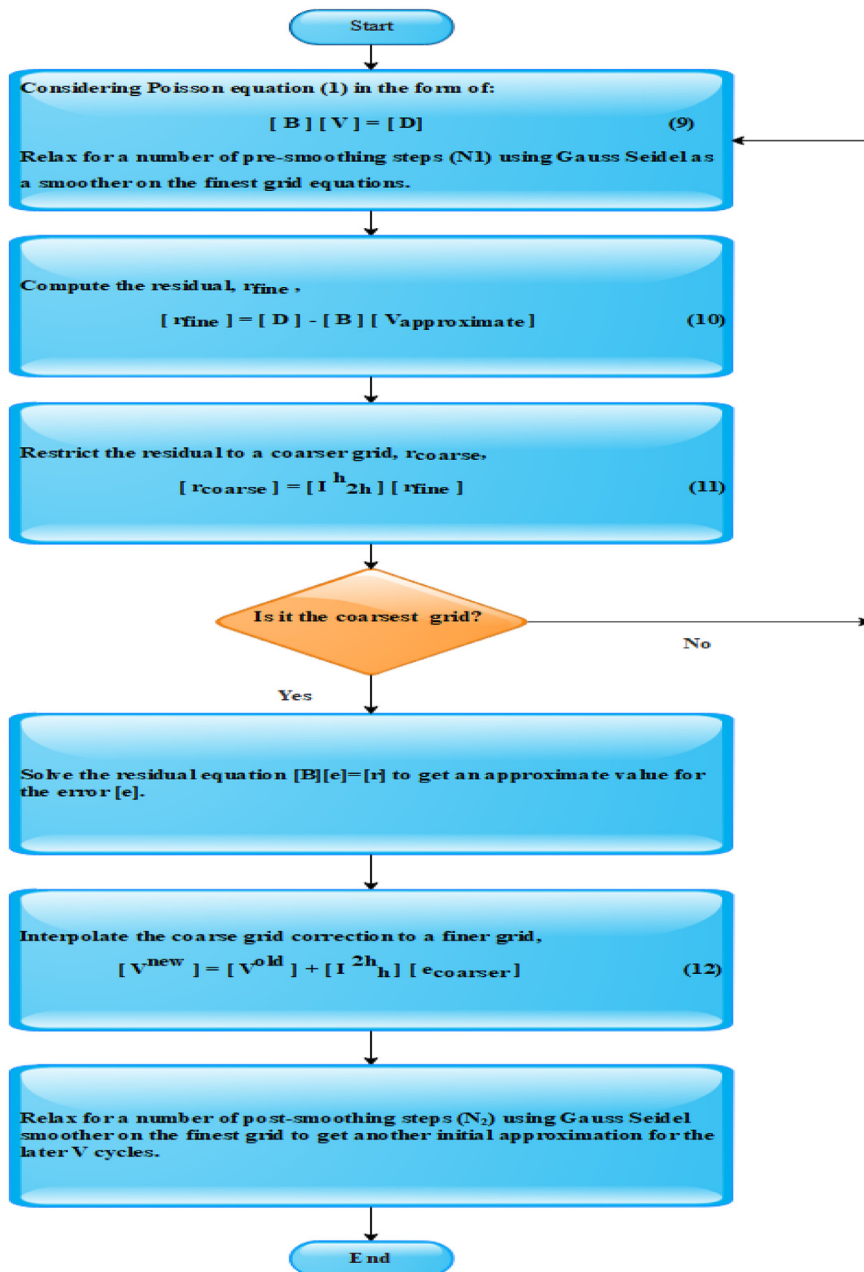


Fig. 2. Partial grid of the intended domain.

$$v_{i,j} \cong (1 - w) v_{i,j} + \frac{w}{2(a_x^2 + a_y^2)} \left( a_x^2(v_{i+1,j} + v_{i-1,j}) + a_y^2(v_{i,j+1} + v_{i,j-1}) + \frac{a_x^2 a_y^2 \rho_{i,j}}{\epsilon_0} \right) \quad (8)$$

Where,  $w$  is a relaxation factor, when  $w = 1$ , successive over relaxation method (SOR) is reduced to Gauss Seidel iterative method.

As mentioned before, the iterative solution is the main reason for consuming excessive time in the overall simulation to reach a certain convergence. Accordingly, Poisson equation takes most of the CPU time. So, Poisson equation will be solved iteratively using the full multigrid method.



$[I_{2h}^h]$ : is the standard full weighting operator.

$[I_h^{2h}]$ : is the bilinear interpolation operator.

Fig. 3. Flowchart of one V-cycle.

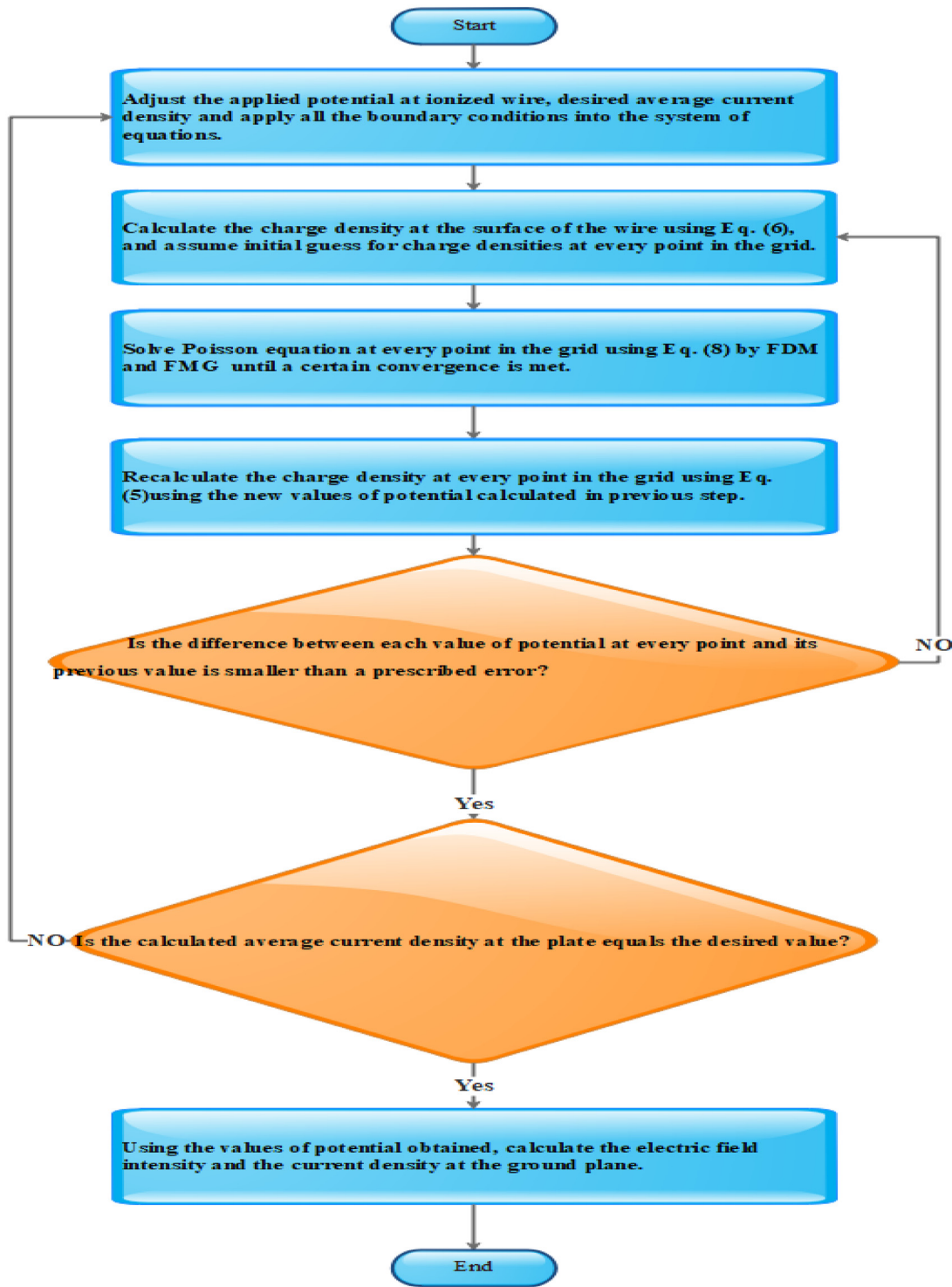


Fig. 4. Flowchart of the computational algorithm.

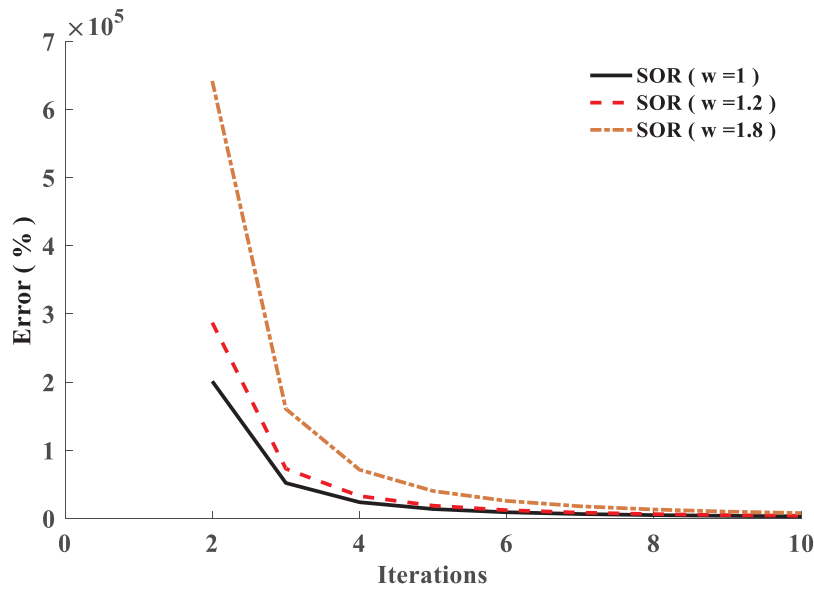
#### 4.1. Full multigrid method

The Full multigrid (FMG) method starts on the coarsest grid and interpolate the solution to the finer grid where several V-cycles are done [2]. Fig. 3 demonstrates the flowchart that summarizes one V-cycle. In the present work, It was found that the number of pre-smoothing steps,  $N_1 = 3$  and the number of post-smoothing steps  $N_2 = 1$ , give the best time performance in the problem.

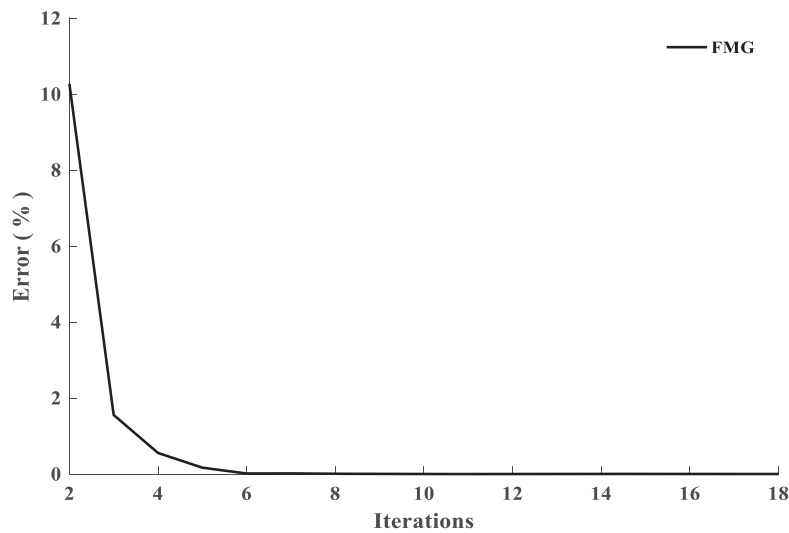
#### 4.2. Computational algorithm

A computer program has been performed in the Matlab environment to solve Poisson and continuity equations. Fig. 4 demonstrates the flowchart that summarizes the proposed method of solution.

$[I_{2h}^h]$ : is the standard full weighting operator.  $[I_h^{2h}]$ : is the bilinear interpolation operator.



(a)



(b)

Fig. 5. Potential error vs. number of iterations by: (a)Successive over relaxation (b) Full Multi-grid Method.

**Table 1**  
The performance of the two methods.

Grid size (129 × 129)	SOR		(FMG)	
	w = 1 (G.S)	w = 1.2	w = 1.8	
Iterations for voltage loop	148,556	103,427	20,380	18
Execution time for voltage loop (sec)	186	129	24	0.2

**5. Results and discussion**

*5.1. Full multi-grid method vs successive over relaxation method*

The most time consuming part in modeling the corona problem is Poisson equation, especially on fine grids. In the present study, Poisson equation is treated by solving the difference equations by successive over relaxation method (SOR), and the full multigrid method (FMG). A comparison between the successive over relaxation method, and the full multigrid method (FMG) is carried out for a Penny and Matick precipitator's geometry of a wire diameter of 2.032 mm, half the spacing

between the two wires,  $S_x$ , equals 7.62 cm, and height of the ionized wire from ground plate,  $S_y$ , equals 11.43cm [29]. The performance of Full Multigrid Method is tested against the successive over relaxation method for a grid size (129 × 129).The convergence of the potential loop is determined such that the percentage error is given by:

$$\%error = \left| \frac{V_{new} - V_{old}}{V_{old}} \right| \times 100 \tag{16}$$

The desired tolerance in the present program equals  $10^{-6}\%$ .

Applying ten iterations in the voltage loop for a grid (129 × 129), the percentage potential error for successive over relaxation method for different relaxation factors (Fig. 5.a), and full multi-grid Method (Fig. 5.b) is computed. The computation is evaluated using Intel (R) Core (TM) i7-3612QM CPU @2.10 GHz.

Table 1 shows the number of iterations and the execution time required by SOR for different relaxation factors and FMG to terminate from the voltage loop by the desired tolerance. In terms of the speeding up factor [2], the successive over relaxation method at  $w = 1.2$  and 1.8 decreases the effort by a factor of 1.4 and 7.3 respectively, compared to

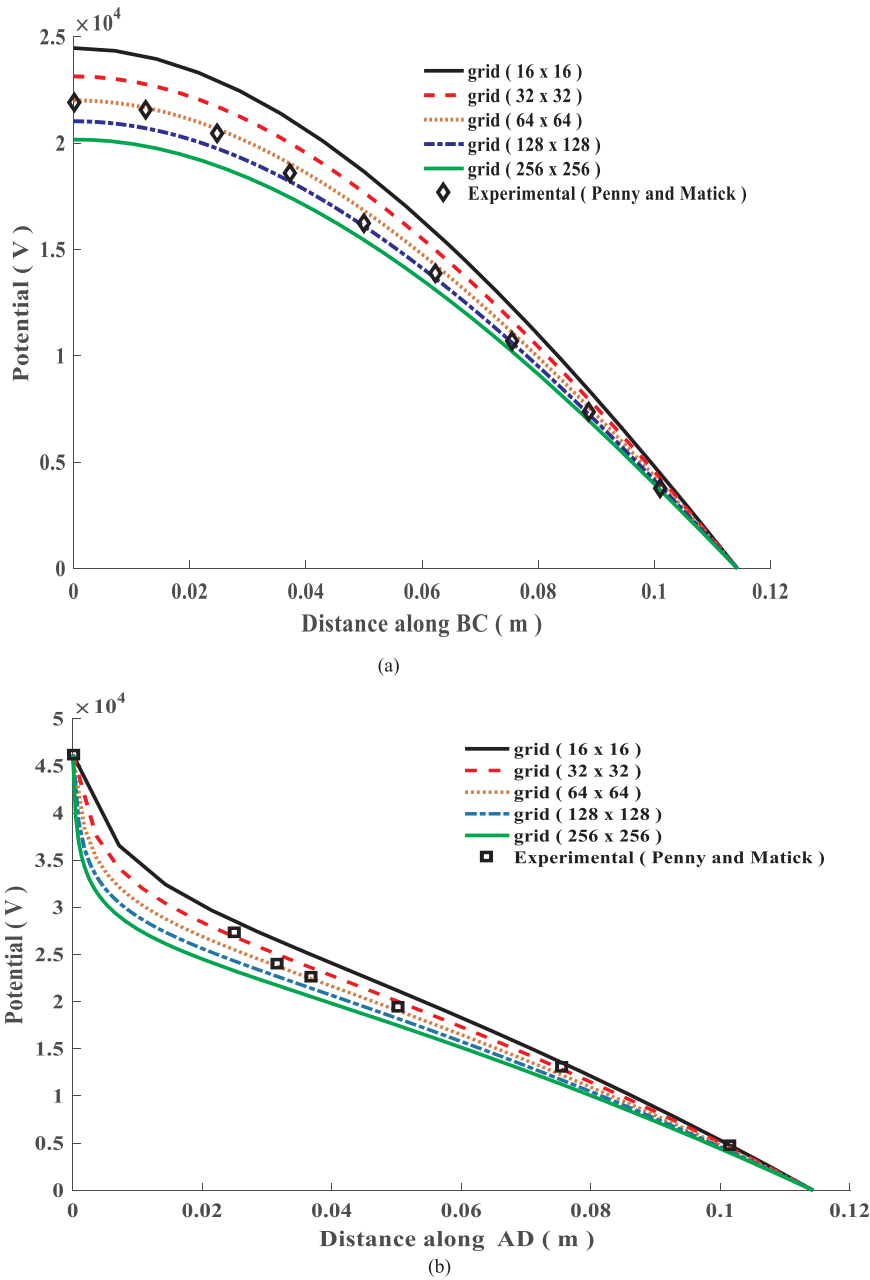


Fig. 6. The potential distribution along the distance: (a) BC (b) AD.

**Table 2**  
Performance of different grid sizes for different applied voltage.

Grid Size	$V = 38.7 \text{ kV}, J_{\text{exp}} = 2.26 \times 10^{-4} \text{ A/m}^2$		$V = 43.5 \text{ kV}, J_{\text{exp}} = 4.84 \times 10^{-4} \text{ A/m}^2$		$V = 46.2 \text{ kV}, J_{\text{exp}} = 6.88 \times 10^{-4} \text{ A/m}^2$	
	$J_{\text{comp}} (\times 10^{-4})$	Error (%)	$J_{\text{comp}} (\times 10^{-4})$	Error (%)	$J_{\text{comp}} (\times 10^{-4})$	Error (%)
(16 × 16)	5.251	132.3	8.037	66	7.92	15
(32 × 32)	2.5357	12	5.268	8.8	7.27	5.66
(64 × 64)	2.3	1.7	4.843	0.06	6.86	0.29
(128 × 128)	2.127	6	4.469	7.6	6.21	9.7
(256 × 256)	1.87	17	4.143	14.4	5.77	16.1

$w = 1$  (Gauss Seidel), while the full multi-grid method decreases the effort by a factor 8253. So, the convergence speed is enhanced in case of full multi-grid method than the successive over relaxation method, which in turn decreases the computational time, not only for the voltage loop but also for the overall numerical procedure implemented in the proposed algorithm. So, we can deal with fine grids without taking

the excessive computational time in mind by using the full multi-grid method.

### 5.2. Choosing the optimal grid for Penny and Matick geometry

In order to choose the optimal grid size that best describes the

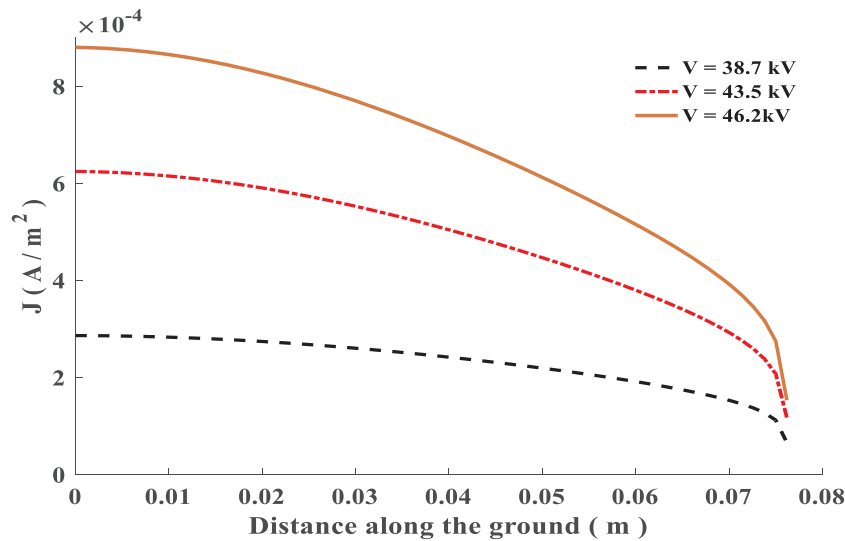


Fig. 7. The current density distribution for different applied voltage.

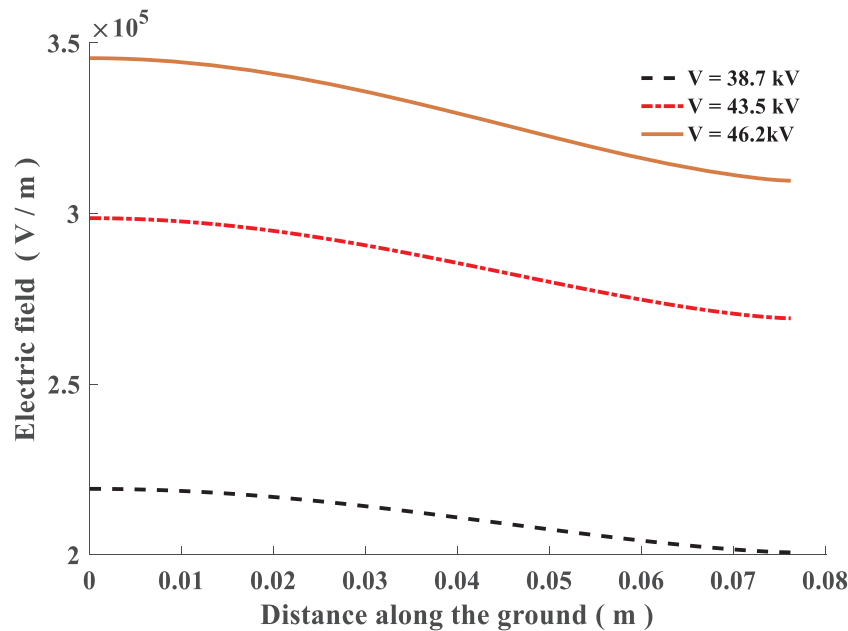


Fig. 8. The Electric field distribution for different applied voltage.

corona problem in precipitators, the finite difference method with the aid of the full multi-grid method as an iterative solver is carried out on different grid sizes up to  $(255 \times 255)$  grid points for Penny and Matick's geometry for precipitator [29]. The effective ion mobility,  $k$ , equals  $1.6 \times 10^{-4} \text{ m}^2/\text{Vs}$ , the applied voltage is 46.2 kV, and the surface roughness factor is taken as 0.75 [2,9].

Fig. 6 demonstrates the calculated potential values along BC and AD for different grid sizes and the measured ones by Penny and Matick. The deviation from the numerical results and the measured ones, for the potential along BC at  $x = 0$ , for a grid sizes of  $(16^2, 32^2, 64^2, 128^2, 256^2)$  is 12%, 6%, 0.4%, 4%, and 8% respectively as shown in Fig. 6.a. It can be pointed out that as the grid becomes finer, the deviation from the experimental results decreases then increases. Firstly, it decreases due to the reduction of the truncation error in the finite difference equations, then increases due to the significant round off errors.

So, the grid size of  $(64 \times 64)$  is the optimal grid for the computational domain for this geometry and this is confirmed by Fig. 6.b, which shows the numerical findings of the grid  $(64 \times 64)$  is the best one that matches the experimental results along AD.

Table 2 compares the difference between the experimental values,  $J_{\text{exp}}$ , of Penny and Matick for the same geometry and the numerical results,  $J_{\text{comp}}$ , for different grid sizes with different applied voltage. The results again confirm that the grid of size  $(64 \times 64)$  is the optimal grid for the computational domain.

Choosing the optimal grid can be an advantage in the early design stage of precipitators, as the designers can figure out and predict the current density and the electrical field on the ground without the need to the experimental efforts which in turn lower the costs.

### 5.3. Prediction of the electric field and current density for different design parameters of Penny and Matick geometry

#### 5.3.1. Variation of applied voltage

Accordingly the effect of the variation of the applied voltage on the current density on the grounded plate for Penny and Matick geometry is illustrated in Fig. 7 using grid  $(64 \times 64)$ . As the applied voltage increases the maximum current density increases as well as the average current density on the plate. The maximum and the average current

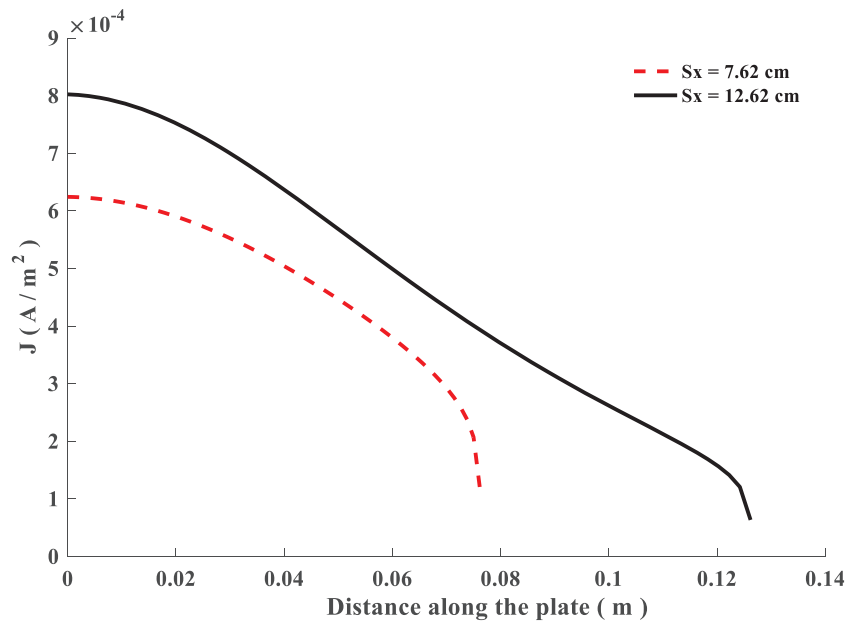


Fig. 9. The current density distribution along the ground for different wire spacing.

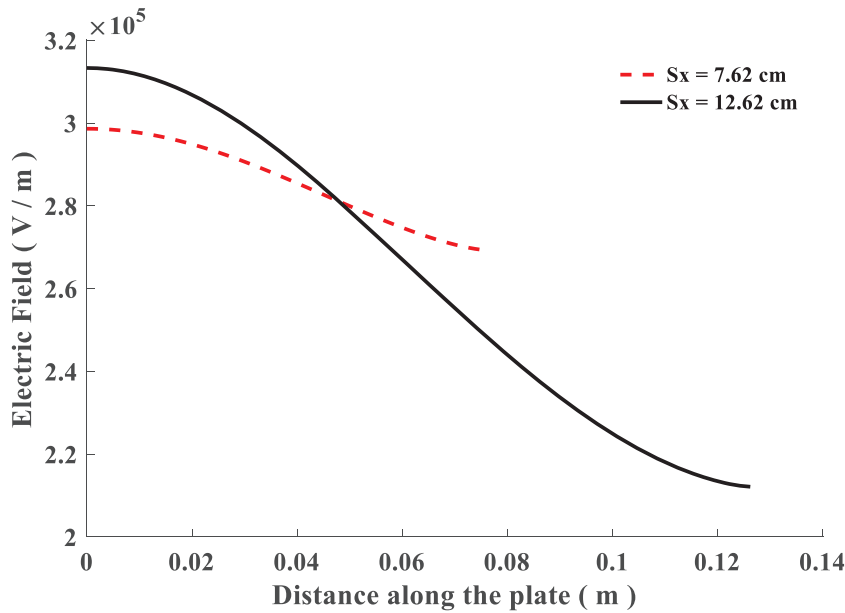


Fig. 10. The electric field distribution along the ground for different wire spacing.

density increases by 207% and 198% respectively when the applied voltage increases from 38.7 kV to 46.2 kV.

Also, the effect of increasing the voltage on the distribution of the electric field on the ground for the same geometry is shown in Fig. 8. As the applied voltage increases from 38.7 kV to 46.2 kV, the maximum electric field increases by 58%.

5.3.2. Variation of the wire to wire spacing

Using the optimal grid (64 × 64) for the above mentioned Penny and Matick geometry, the effect of changing the wire to wire spacing on the current density distribution on the ground plate is studied as shown in Fig. 9. As the wires get closer to each other, the corona onset voltage increases resulting in lower current density at the same applied voltage. The maximum current density increases by 28.5% as the half spacing between wires,  $S_x$ , increases from 7.62 cm to 12.62 cm at 43.5 kV.

In addition, the effect of altering the wire to wire spacing on the

electric field distribution on the ground plate is shown in Fig. 10 at 43.5 kV. It is pointed out that the two electric field distribution for spacing 7.62 and 12.62 cm cross each other at  $x = 0.05$  m. Before the cross over point, the electric field intensity is higher for spacing of 12.62 cm, then after it, the electric field for the spacing of 7.62 cm starts to increase with values higher than that of the spacing 12.62 cm. This phenomenon may be attributed to that as the two wires get closer to each other, the overlapping area between two wires increases for a voltage above the corona onset voltage for both spacing.

5.3.3. Variation of the wire height

For the same geometry, the effect of changing the wire height on the current density distribution on the ground plate is shown in Fig. 11 at 43.5 kV using grid (64 × 64). As the wires get closer to the ground, the corona onset voltage of the wire decreases resulting in higher current density at the same applied voltage. The maximum current density

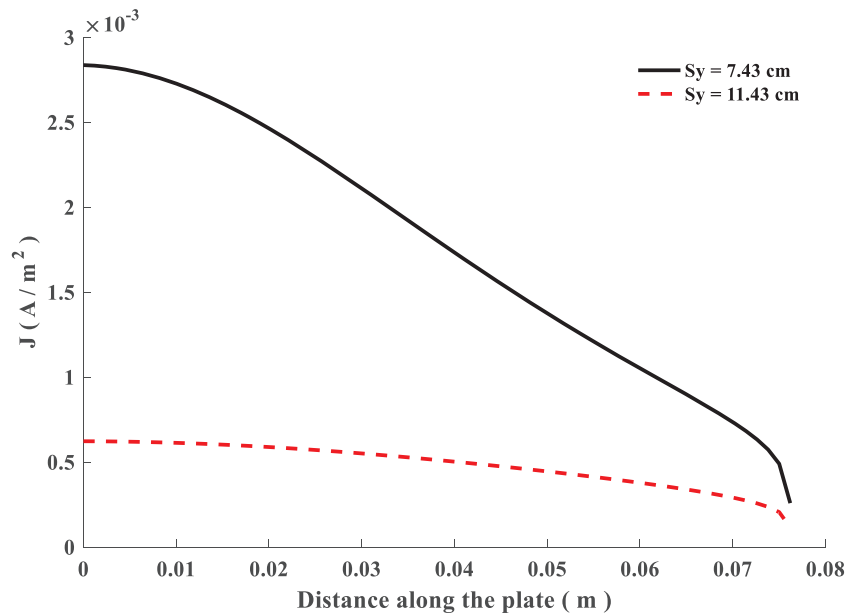


Fig. 11. The current density distribution along the ground for different wire height.

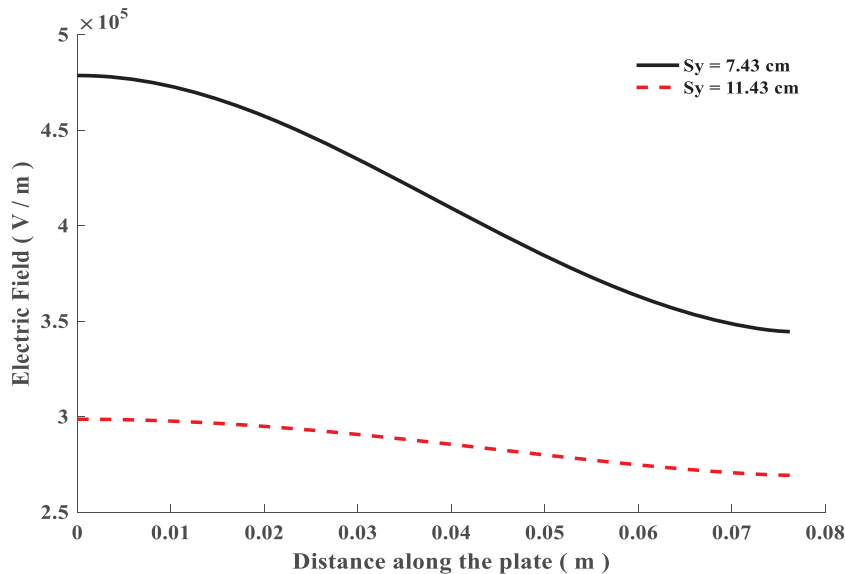


Fig. 12. The electric field distribution along the ground for different wire height.

increases by 345.5% as the wire height,  $S_y$ , decreases from 11.43 cm to 7.43 cm. Also, it is noted that as the height of wire increases, the region exposed to current density almost the same.

The effect of altering the wire height on the electric field distribution on the ground plate is assessed in Fig. 12 at 43.5 kV. As the wire height above the ground increases, the electric field intensity decreases. The maximum electric field intensity increases by 60% as the wire height, decreases from 11.43 cm to 7.43 cm.

Generally, changing the spacing between wires and the wire height affects the current density and electric field distributions above the grounded plate, but their values is critical as it is constrained to the overall size of the precipitator.

#### 5.4. Choosing the optimal grid for Tassicker geometry and Felici geometry

To confirm the effectiveness of the full multi-grid method in choosing the optimal grid size, the finite difference method with the full multi-grid method is carried out on different grid sizes up to 2552 grid

points for Tassicker geometry for precipitator [30]. Tassicker implemented a microprobe for accurate current density measurement at the grounded plate. The wire has a diameter of 0.3 mm; the wire to wire spacing is 10 cm and is hanged at distance 11.5 cm from the ground. The surface roughness factor,  $f$ , equals unity, and the ion mobility,  $k$ , equals  $1.8 \times 10^{-4} \text{ m}^2/\text{Vs}$  [30].

For instance, the percentage error from the measured ones, for the current density at  $x = 0$ , for a grid sizes of  $(16^2, 32^2, 64^2, 128^2, 256^2)$  is 23.5%,13%,5%,1.4%, and 7% respectively. So, the optimal grid size for Tassicker geometry is  $(128 \times 128)$ , as shown in Fig. 13.

Also, the proposed method is applied for Felici geometry for various grid sizes at applied voltage 31 kV. The design parameters are: wire radius of 0.127 mm,  $S_x$  and  $S_y$  equal 0.05 m and 0.1 m respectively, the ion mobility is taken as  $1.8 \times 10^{-4} \text{ m}^2/\text{Vs}$  [31]. The computed current density for a grid sizes  $(16^2, 32^2, 64^2, 128^2, 256^2)$  deviated by 12%,1%,6%,12%, and 16% respectively from the experimental values at  $x = 0$  as shown in Fig. 14. So, the optimal grid size for Felici geometry is  $(32 \times 32)$ , as shown in Fig. 14.

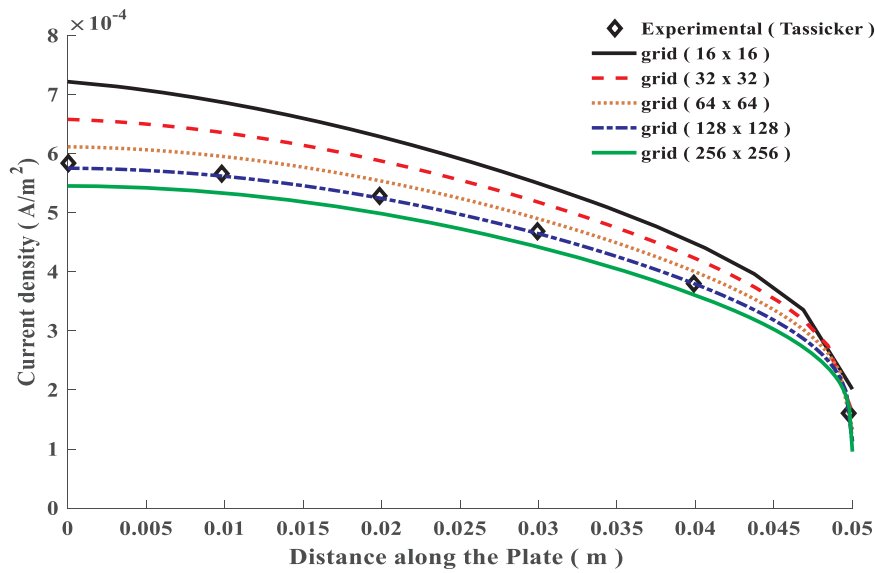


Fig. 13. The current density distribution along the plate.

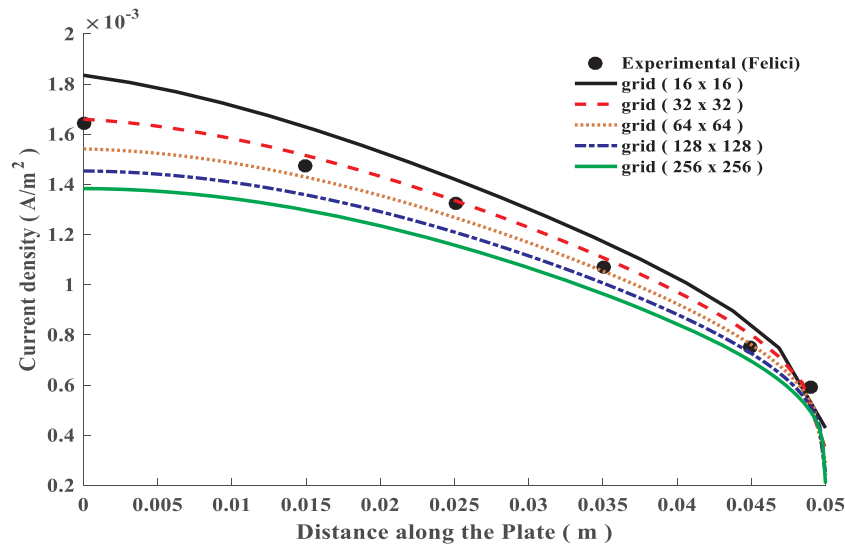


Fig. 14. The variation of the current density along the plate.

Again, as the grid size gets finer, the numerical findings approaches the experimental results till they fit each other, then they deviate from each other. Accordingly, the tracking of the optimal grid grants lower truncation error and round off error.

**6. Conclusion**

Choosing the optimal grid by using the finite difference method integrated with the full multi-grid on finer grids was presented in the paper. This would help a lot in getting an accurate picture about the electrical conditions of the precipitators and can be more confident about the predictions of the numerical outcomes, without the need of the costly experiments. The full multi-grid method was compared to the successive over relaxation method for different relaxation factors and the full multi-grid method succeeded as it enhances the convergence rate of the Finite Difference Method, especially on finer grids. Unlike the other proposed techniques, firstly, the finite difference method with the aid of the Full Multigrid method is free to work on fine computational domains without taking in mind the problem of excessive computational time especially on solving Poisson equation in the ionized field problem. Secondly, the proposed algorithm is able to track the

optimal grid for the computational domain for a certain design of precipitator, without the need for the costly experiments, so, it can be an effective tool for the engineers in the design stage. Thirdly, the proposed technique best fit the experimental results than the other proposed techniques. The proposed method was implemented on different designs of precipitators, and an optimal grid was reached, which grants both low truncation error and round off error. After, reaching the optimal grid for a certain design, this grid was used to predict the distribution of the current density and electric field as a result of different design parameters like applied voltage, wire-wire spacing and the wire height above the grounded plate.

**CRedit authorship contribution statement**

**Mohamed A. Abouelatta:** Conceptualization, Methodology, Validation, Supervision, Investigation, Data curation, Writing - original draft, Writing - review & editing, Visualization. **A.M. Omar:** Methodology, Software, Formal analysis, Investigation, Data curation, Writing - original draft, Writing - review & editing, Visualization. **Sayed Ward:** Supervision, Writing - review & editing, Project administration.

## Declaration of Competing Interest

None.

## References

- [1] I.V. Muralikrishna, V. Manickam, Air pollution control technologies, Environmental Management Science and Engineering for Industry, Elsevier, 2017, pp. 337–397.
- [2] O. Ahmad Muhammed, M.A. Abouelatta, Fast corona discharge solver for precipitators using multi-grid methods on fine grids, IET Science, Measurement & Technology 133 (2018) 453–460.
- [3] D.A. Vallerio, Air pollution control technologies, Fundamentals of Air Pollution, 5th Edition, Academic press, 2014, pp. 829–879.
- [4] K. Parker, Electrical Operation of Electrostatic Precipitators, IET, 2003.
- [5] J. Hammerschmidt, J. Güntner, B. Kerstiens, A. Charitos, Roasting of gold ore in the circulating fluidized-bed technology, Gold Ore Processing, Second Edition, Elsevier, 2016, pp. 393–409.
- [6] N. Ahern, Mercury in gold processing, Gold Ore Processing, 2nd Edition, Elsevier, 2016, pp. 753–766.
- [7] C.D. Tsadilas, E. Evangelou, Coal fly ash utilization for boron management in soils, plants, and waters, Environmental Materials and Waste, Academic Press, 2016, pp. 647–663.
- [8] H. Lei, L.-Z. Wang, Z.-N. Wu, Applications of upwind and downwind schemes for calculating electrical conditions in a wire-plate electrostatic precipitator, J. Comput. Phys. 193 (2) (2004) 697–707.
- [9] J.R. McDonald, et al., A mathematical model for calculating electrical conditions in wire-duct electrostatic precipitation devices, J. Appl. Phys. 48 (6) (1977) 2231–2243.
- [10] G.A. Kallio, D.E. Stock, Computation of electrical conditions inside wireduct electrostatic precipitators using a combined finite-element, finite-difference technique, J. Appl. Phys. 59 (6) (1986) 1799–1806.
- [11] K. Adamiak, Simulation of corona in wire-duct electrostatic precipitator by means of the boundary element method, IEEE Trans. Ind. Appl. 30 (2) (1994) 381–386.
- [12] B.S. Rajanikanth, N. Thirumaran, Prediction of pre-breakdown V-I characteristics of an electrostatic precipitator using a combined boundary element-finite difference approach, Fuel Process. Technol. 76 (3) (2002) 159–186.
- [13] M. Abdel-Salam, A. Eid, Finite element simulation of corona in wire-duct precipitators, Industry Applications Conference. 37th IAS Annual Meeting, USA, 2002.
- [14] A.A. Elmoursi, G.S. Peter Castle, Modeling of corona characteristics in a wire-duct precipitator using the charge simulation technique, IEEE Trans. Ind. Appl. 1 (1987) 95–102.
- [15] Z. Al-Hamouz, A. El-Hamouz, N. Abuzaid, Simulation and experimental studies of corona power loss in a dust loaded wire-duct electrostatic precipitator, Adv. Powder Technol. 22 (6) (2011) 706–714.
- [16] Z.M. Al-Hamouz, A combined algorithm based on finite elements and a modified method of characteristics for the analysis of the corona in wire-duct electrostatic precipitators, IEEE Trans. Ind. Appl. 38 (1) (2002) 43–49.
- [17] J.L. Davis, J.F. Hoburg, Wire-duct precipitator field and charge computation using finite element and characteristics methods, J. Electrostat. 14 (2) (1983) 187–199.
- [18] N. Neimarlija, I. Demirdžić, S. Muzaferija, Finite volume method for calculation of electrostatic fields in electrostatic precipitators, J. Electrostat. 67 (1) (2009) 37–47.
- [19] Z. Long, et al., A second-order accurate finite volume method for the computation of electrical conditions inside a wire-plate electrostatic precipitator on unstructured meshes, J. Electrostat. 67 (4) (2009) 597–604.
- [20] Briggs, W.L., and Steve F. McC "A multigrid tutorial" 2000, 72.
- [21] T. Guillet, T. Romain, A simple multigrid scheme for solving the Poisson equation with arbitrary domain boundaries, J. Comput. Phys. 230 (12) (2011) 4756–4771.
- [22] F. Gibou, et al., A second-order-accurate symmetric discretization of the Poisson equation on irregular domains, J. Comput. Phys. 176 (1) (2002) 205–227.
- [23] F.W. Peek, Dielectric Phenomena in H. V. Engineering, Mc Graw Hill, 1929, pp. 52–80.
- [24] M. Abdel-Salam, M. Nakano, A. Mizuno, Corona-induced pressures potentials fields and currents in electrostatic precipitator configurations, J. Phys. D 40 (2007) 1919–1926.
- [25] Y. Zheng, J. He, B. Zhang, R. Zeng, Z. Yu, Photoemission replenishment criterion for inception of negative corona discharges in air, IEEE Trans. Power Deliv. 26 (3) (2011) 1980–1987.
- [26] P.N. Mikropoulos, V.N. Zagkanas, Threshold inception conditions for positive DC corona in the coaxial cylindrical electrode arrangement under variable atmospheric conditions, IEEE Trans. Dielectr. Electr. Insul. 22 (1) (2015) 278–286.
- [27] Y. Zheng, B. Zhang, J. He, Self-sustained criterion with photoionization for positive dc corona plasmas between coaxial cylinders, Phys. Plasmas 22 (2015) 063514.
- [28] P.N. Mikropoulos, V.N. Zagkanas, Negative DC corona inception in coaxial cylinders under variable atmospheric conditions: a comparison with positive corona, IEEE Trans. Dielectr. Electr. Insul. 23 (3) (2016) 1322–1330.
- [29] G.W. Penney, R.E. Matick, Potentials in DC corona fields, Trans. Am. Inst. Electr. Eng. Part I 79 (2) (1960) 91–99.
- [30] O.J. Tassicker, Measurement of corona current density at an electrode boundary, Electron. Lett. 13 (5) (1969) 285–286.
- [31] N.J. Felici, Recent advances in the analysis of the DC ionized fields-Part II, Direct Curr. 8 (1963) 278–287.